Ultrafast Magnetoacoustics in Nickel Films

Ji-Wan Kim, Mircea Vomir, and Jean-Yves Bigot*

Institut de Physique et Chimie des Matériaux de Strasbourg, UMR 7504, CNRS, Université de Strasbourg, BP 43, 23 rue du Loess, 67034 Strasbourg Cedex 02, France

(Received 30 November 2011; published 17 October 2012)

We report about the magnetization dynamics of a ferromagnetic nickel film at room temperature excited by acoustic pulses generated with femtosecond laser pulses. The ultrafast change of magnetization is detected from both the front and back sides of the nickel film. The propagating strain associated with the acoustic pulses modifies the magnetic anisotropy and induces a precession of the magnetization. We model the time-dependent magnetoacoustic response of the metallic film by combining a three temperature model for the temperatures of the charges, the spins, and the lattice, the wave equation for the strain, and the Landau-Lifshitz-Gilbert equation for the magnetization. It is shown that the precession dynamics can be controlled by matching the precession period with the round trip time of the acoustic echoes. The calculation of the time-dependent precession torque $\tau = |M \times H_{\text{eff}}|$ allows understanding the underlying physics.

DOI: 10.1103/PhysRevLett.109.166601 PACS numbers: 72.55.+s, 75.78.Jp, 78.20.hc, 78.20.Ls

The technology of information and communication constantly needs to improve the speed and density of memory devices. Towards that goal, intense research is being carried out for manipulating the spin in magnetic materials using various excitation methods like the use of external magnetic field pulses [1–3]. Alternatively, femtosecond laser pulses have been utilized to induce an ultrafast demagnetization [4–10] or the inverse Faraday effect [11,12]. This new field of magnetism, named ''femtomagnetism'' [13–15], uses photons to directly manipulate magnetic structures with a temporal resolution of a few femtoseconds. The demagnetization can then be used to modify the anisotropy of the magnetic material [16] which leads to a reorientation of the magnetization vector followed by its precession and damping [7,17,18]. Sherbakov *et al.* have shown an alternative way of controlling the magnetization using picosecond acoustic pulses in a ferromagnetic semiconductor at 1.6 K [19]. Acoustic pulses in metals and semiconductors have been extensively studied [20–26] and their extension to ferromagnetic systems is very promising for applications. Indeed for ferromagnetic metals, it is worthwhile manipulating the magnetization at room temperature over a few hundreds of nanometers as it corresponds to the typical distance for the propagation of surface plasmon polaritons in nanostructures [27].

In the present work we explore the magneto-optical dynamics measured at the front and back sides of a ferromagnetic Ni film at room temperature. We show that the acoustic pulses induce a transient reorientation and a precession of the magnetization which is controlled by modifying the torque. Our results are well explained by using three dynamical equations describing the temperatures of three baths (T_e: electrons, T_s: spins, and T_l: lattice), the strain, and the magnetization dynamics. The primary goal is not about the generation of the acoustic pulses, already very well known in metals and semiconductors [20–25], but we studied it with details for the quantitative modeling of magnetoacoustic effects.

The experiment consisted in generating longitudinal acoustic waves from the front side of Ni with femtosecond pump pulses (150 fs, 397 nm) and detecting the dynamics on both sides of the film with probe pulses p_{front} and p_{back} (120 fs, 794 nm), using the time-resolved magneto-optical Kerr effect. They are focused onto the sample within a spot diameter (200 μm) twice larger than the two probe beams. The reflectivity $R(t)$, polarization rotation $\theta(t)$, and ellipticity $\varepsilon(t)$ of both sides of the sample are probed with polarization bridges as a function of the pump and probe delay time t. We used a polycrystalline 200 nm thick Ni film, deposited either on a glass or on a sapphire substrate by electron-beam evaporation.

Figure 1 shows the differential reflectivity $\Delta R(t)/R_s$ on the front [Fig. 1(a)] and back [Fig. 1(b)] sides of the Ni/glass for a pump energy density $I_p = 1.7\ \text{mJ cm}^{-2}$. For p_{front}, in addition to the well-known thermal dynamics associated with a heating of the electrons and lattice, four acoustic echoes with a period of $T = 98$ ps are observed. For p_{back} $\Delta R(t)/R_s$ shows echoes and oscillations for Ni/glass. These oscillations are due to interferences between the probe beam reflected at the Ni-glass interface and secondary beams reflected by the strain pulse propagating in the substrate [28]. They disappear for Ni/sapphire [dotted line in Fig. 1(b)] because Sapphire has a negligible piezo-optic coupling at 800 nm [22].

We model $\Delta R(t)/R_s$ by taking into account the dynamical changes of the thermo-optic and piezo-optic properties affecting the complex refractive index $\tilde{n}$ as follows: $\Delta\tilde{n} = \frac{\partial\tilde{n}}{\partial T_e}\Delta T_e + \frac{\partial\tilde{n}}{\partial\eta}\Delta\eta$, where $\eta(z,t)$ is the strain and z the direction of propagation perpendicular to the film surface. The partial derivatives are the thermo-optic and piezo-optic

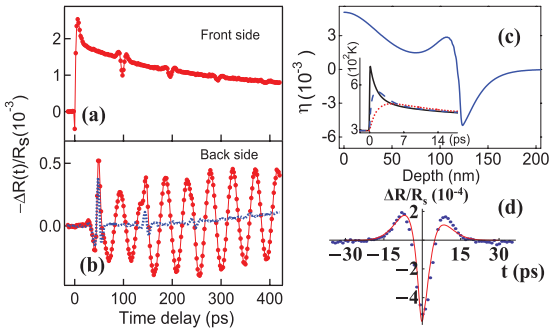

FIG. 1 (color). Dynamics of reflectivity and strain on 200 nm thick Ni sample. (a) $\Delta R(t)/R_s$ on the front side of Ni. (b) $\Delta R(t)/R_s$ on the back side of Ni/glass (closed circle) and Ni/sapphire (dotted curve). (c) Modeling of the strain profile at $t = 30$ ps. Inset: electron (full), spin (dashed), and lattice (dotted) temperatures profiles calculated with Eq. (1). (d) Fit of $\Delta R(t)/R_s$ on the front side of Ni/glass using the model.

coefficients, respectively. The thermo-optic part involves $\Delta T_e(z, t)$ [29], while the piezo-optic part occurs via $\frac{\partial T_l(z,t)}{\partial t}$ [21]. As we are ultimately interested in the magnetoacoustic response, we add $T_s(z, t)$ and solve the following coupled temperature equations:

$$C_i(T_i)\frac{\partial T_i}{\partial t} = \delta_{ie}\left[\frac{\partial}{\partial z}\left(\kappa_i \frac{\partial T_i}{\partial z}\right) + P(z, t)\right] - g_{ij}(T_i - T_j), \tag{1}$$

where $i, j = e, l, s$ stand for electrons, lattice, and spins and δ_{ie} is the Kronecker symbol. C_i and κ_i are the heat capacity per unit volume and the thermal conductivity of bath i. $g_{ij}(= g_{ji})$ is the coupling constant between two baths i and j, and $P(z, t)$ the laser source term. The parameter values which we used are listed in Ref. [30]. We first obtain $T_l(z, t)$ from Eq. (1) [dotted line in the inset of Fig. 1(c)]. This is taken into account in computing the following one-dimensional wave equation [21].

$$\rho\frac{\partial^2 u(z, t)}{\partial t^2} = \rho v^2 \frac{\partial^2 u(z, t)}{\partial z^2} - 3\beta B\frac{\partial \delta T_l}{\partial z}. \tag{2}$$

u ($\eta = \partial u/\partial z$) is the lattice displacement, ρ the mass density, v the sound velocity, β the linear thermal expansion coefficient, and B the bulk modulus of Ni. The full strain profile obtained with Eq. (2) for $t = 30$ ps is shown in Fig. 1(c). It consists of a quasistationary part near the surface of the film and a propagating part which is partially transmitted to the substrate and partially reflected back to the film with a reflection coefficient $r_{ac} \sim -0.39$, obtained from successive echoes in Fig. 1(a). For the forward propagation of the strain pulse the tensile part arrives first at the film surface, while for the backward propagation the compressive part arrives first at the Ni-glass interface. Therefore, the sign of the echoes are reversed on the front side [Fig. 1(a)] and back side [Fig. 1(b)]. Figure 1(d) shows the differential reflectivity calculated (full line) with the strain pulse of Fig. 1(c) and Eq. (6) in Ref. [25], together with the experimental result (dots). This good quantitative agreement is the primary step to understand and simulate the magnetoacoustic dynamics described in the following.

Let us now focus on the ultrafast magnetoacoustic properties of Ni. To investigate the effect of the coupling between the strain pulse and the magnetization, we measured the differential magneto-optical Kerr response $\Delta\theta/\theta_s$ and $\Delta\varepsilon/\varepsilon_s$ from the front side [Figs. 2(a) and 2(b)] and back side [Figs. 2(c) and 2(d)] for two angles of the static magnetic field $\phi = 25°$ and 45°, with respect to the normal to the sample. The pump excitation is $I_p = 2.0$ for Fig. 2(a) and 1.7 mJ cm^{-2} for Figs. 2(b)–2(d). The oscillations correspond to a precession of the magnetization around the effective field as already reported in several ferromagnetic materials [7,16–18]. It results from the initial demagnetization of the Ni film induced by the pump pulse which occurs within the thermalization time of the spins [6]. Two weak magnetoacoustic pulses show up at the same delays T and $2T$ as those present on the reflectivity curves [Fig. 1(a)]. It shows that the acoustic pulse induces a modification of the magnetocrystalline anisotropy as mentioned by Scherbakov *et al.* [19]. The magnetoacoustic echoes are more contrasted on $\Delta\varepsilon/\varepsilon_s$ [Fig. 2(b)] where they are observed up to $t = 3T$.

Figures 2(c) and 2(d) show the dynamic signals on the back side of the film $\Delta\theta/\theta_s$ and $\Delta\varepsilon/\varepsilon_s$ for $\phi = 25°$ and 45°. Note that the static Faraday contribution due to the substrate has been removed. In contrast to the front side measurements [Figs. 2(a) and 2(b)], the precession is now induced only by the strain pulse. The magnetization is first brought out of equilibrium by the strain pulse when it arrives on the back side of the film at $T/2$, initiating the motion of precession. Similarly to the reflectivity echoes [Fig. 1(a)], subsequent echoes of magnetoacoustic pulses

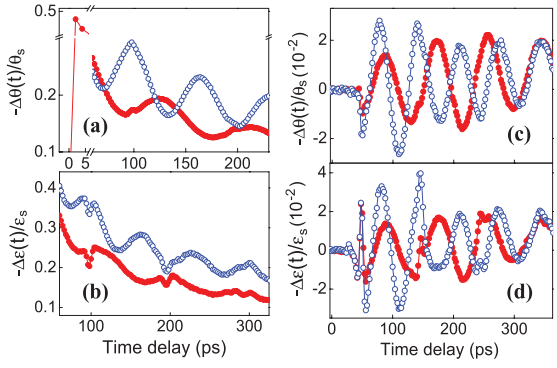

FIG. 2 (color). Differential Kerr rotation $\Delta\theta/\theta_s$ (a) and ellipticity $\Delta\varepsilon/\varepsilon_s$ (b) probed on the front side of Ni/glass for $\phi = 25°$ (closed circle) and 45° (open circle). The temporal scale is cut on (a) to better show the early demagnetizing signal and the curves on (a) and (b) are shifted along the ordinate axis for clarity. (c) and (d) same quantities probed on the back side of Ni/glass.

occur at $(2m+1)T/2$, $(m=1,\ 2)$. They are also much better contrasted on $\Delta\varepsilon/\varepsilon_s$.

Three main temporal features are present in the dynamics of the rotation and ellipticity: the sharp magnetoacoustic echoes, the dynamics of precession, and an overall slow increase of the signal. First, the sharp echoes are directly induced by the strain pulse. Therefore, the corresponding temporal shape is similar to that of strain echoes as shown in Fig. 3(a). Second, the motion of precession results from a dynamical change of the magnetic anisotropy. From that point of view the relative amplitude of the effect is similar on $\Delta\theta/\theta_s$ and $\Delta\varepsilon/\varepsilon_s$. Third, the slow increase of the rotation and ellipticity at long time delays (several hundreds of picoseconds) is due to a slow increase of the strain due to the temperature increase associated with the thermal diffusion within the film depth.

Regarding the sharp magnetoacoustic echoes, their difference of amplitude in the rotation and ellipticity signals results from the difference of the real and imaginary parts of the magneto-optical response upon exerting the strain. More specifically, the real and imaginary parts of the linear magneto-optical response, which are related by Kramers-Kronig relations, are usually different due to the particular band structure of the material [34]. When modifying the lattice parameter their local spectral shapes may differ (for example, due to the shift and broadening of the resonances associated with the interband transitions). In the case of Ni at 1.5 eV the static rotation $\theta(\omega)$ is almost flat while $\varepsilon(\omega)$ has a slope [35]. Consequently, under the dynamical strain, $\Delta\theta(t)/\theta$ varies much less than $\Delta\varepsilon(t)/\varepsilon$.

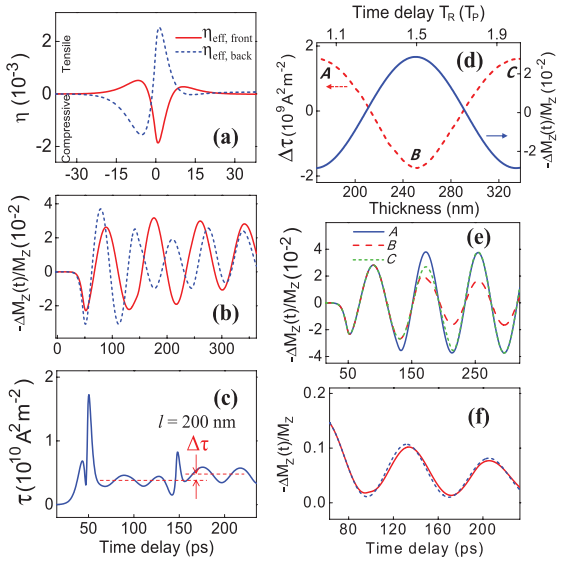

FIG. 3 (color). Modeling of magnetoacoustic response. (a) Effective strain pulse profiles at the front side (full curve) and back side (dashed curve). (b) $\Delta M_z/M_z$ for $\phi = 25°$ (full curve) and 45° (dashed curve). (c) $\Delta\tau$ induced by the acoustic echoes for $l = 200$ nm Ni/glass. (d) Dashed curve: $\Delta\tau$ calculated as a function of l (bottom abscissa) or round trip time T_R (top abscissa). Full curve: $\Delta M_z/M_z$ calculated for $l = 200$ nm and $\phi = 25°$ as a function of time (expressed in numbers of round trip time T_R, top abscissa). (e) $\Delta M_z/M_z$ for 3 round trip times T_R (or sample thicknesses l) corresponding to the points (A, B, and C) in Fig. 3(d). (f) $\Delta M_z/M_z$, on the front side, calculated with (full curve) and without (dashed curve) acoustic echoes for $l = 200$ nm and $\phi = 25°$.

To model the magnetoacoustic dynamics quantitatively we use the Landau-Liftshitz-Gilbert equation [36] taking into account the effect of the strain pulse.

$$\frac{dM}{dt} = -\gamma\mu_0(M \times H_{\text{eff}}) + \frac{\alpha}{M_s}\left(M \times \frac{dM}{dt}\right). \qquad (3)$$

γ is the gyromagnetic ratio, H_{eff} the effective magnetic field, and α Gilbert damping parameter. We consider the magnetoelastic energy equation: $E_{\text{me}} = -3/2\lambda_s\sigma_s\cos^2\varphi$, where λ_s is the magnetostriction coefficient of a polycrystalline Ni, $\sigma_s = 3(1-\nu)/(1+\nu)B\eta$ the stress [24], ν the Poisson's ratio, and φ the angle between the strain direction and the magnetization vector. We choose an effective strain pulse η_{eff}, which takes into account the reflected pulse η_{ref}, the incoming strain pulse η_{inc}, and the absorption length ζ of the probe beam. The effective strain is then given by: $\eta_{\text{eff}}(t) = \frac{1}{\zeta}\int_0^\infty e^{-(z/\zeta)}[\eta_{\text{inc}}(z+vt) + \eta_{\text{ref}}(z-vt)]dz$, where $\eta_{\text{ref}} = r_{\text{ac}}\eta_{\text{inc}}$. By using the strain pulse profile obtained from Fig. 1(c), the two effective strain pulses on both sides of the film are shown in Fig. 3(a). The full curve stands for the 1st order echo on the front side and the dashed one represents the 0th order echo on the back side at $t = T/2$. Here, + and − values signify tensile and compressive parts of the pulses, respectively. The main features of the magnetization dynamics on the back side are well reproduced for $\phi = 25°$ and 45° as seen in Fig. 3(b). The calculated quantity is the differential magnetization $\Delta M_z/M_z$ projected on the z axis. As it is well known in linear magneto-optics, M_z is proportional to θ_s and ε_s. The precession dynamics as well as the temperature at the back side continuously increases like in the experimental results (Fig. 2). From the three temperatures model calculation the corresponding temperature raise is ~10 K at $t = 300$ ps.

Importantly, one can control the magnetization dynamics by an appropriate choice of the echo period T and the period of the precession T_P. To model such an effect we extract from Eq. (3) the torque $\tau = |M \times H_{\text{eff}}|$. Due to the strain, the torque τ changes for a given sample thickness l as shown in Fig. 3(c). For each echo, τ presents a maximum due to the strain and then oscillates around an average value. We define the change of torque $\Delta\tau$ as the difference between the average value after the 0th and 1st order echoes [see Fig. 3(c)]. To see the influence of the torque on the precession dynamics, we then calculate $\Delta\tau$ as a function of the sample thickness l [dashed curve in Fig. 3(d)], which is proportional to the round trip time T_R of the echo ($T_R = 2l/v$). On Fig. 3(d) we compare $\Delta\tau$ to the precession dynamics $\Delta M_z/M_z$ [full curve in Fig. 3(d)]

for a fixed sample thickness $l = 200$ nm (like in the experiment), where the arrival time of the 0th order echo is set as a zero for comparison with T_R. Clearly the maximum change of $\Delta\tau$ occurs when the echo arrives in a minimum of the precession $\Delta M_z/M_z$, that is, $T_R = mT_P$, $(m = 1, 2, \ldots)$. On the contrary $\Delta\tau$ is minimum when the echo coincides with a maximum of precession, that is, $T_R = (2m - 1)T_P/2$. Therefore, depending on the ratio T_R/T_P between the round trip time of the echo and the precession period, one can enhance or decrease the amplitude of the oscillations. This is shown in Fig. 3(e) where the precession dynamics is shown for the three points (A, B, and C) pointed out in Fig. 3(d), the sample thickness being set at 200 nm. Instead of changing the sample thickness to act on T_R one can modify T_P by changing the angle ϕ of the magnetic field as we did in the experiment (see Fig. 2). $\Delta\tau$ can also be controlled with r_{ac} by choosing appropriate interfaces. For example, the change of precession by the 1st order echo on the front side is not as prominent as on the back side because of different r_{ac} as seen in Fig. 3(f) showing $\Delta M_z/M_z$ in the presence (full curve) and absence (dashed curve) of the strain echo. Our analysis on the precession torque shows that a particular sequence of strain pulse echoes allows manipulating the precession dynamics, either by reducing or increasing the amplitude of the oscillations. This new effect could be used either to realize a magnetoacoustic modulator or to switch a thin soft magnetic layer deposited on a thick hard magnetic one excited by the femtosecond laser pulses.

In conclusion, we have studied the magnetoacoustic dynamics in a nickel film excited with femtosecond laser pulses at room temperature. We have shown that the acoustic pulse propagation to the back side of the film modifies the magnetoelastic energy due to the large lattice deformation. It induces a motion of precession which can be controlled by matching the round trip time of the strain pulse echoes with the period of precession. Our model accounts quantitatively for the observed magnetization dynamics and manipulation of the precession. These results open a new way of controlling magnetoacoustic devices at room temperature.

The authors acknowledge the financial support of the European Research Council with the ERC Advanced Grant ATOMAG (ERC-2009-AdG-20090325 247452).

*bigot@ipcms.u-strasbg.fr

[1] Y. Acremann, C. H. Back, M. Buess, O. Portmann, A. Vaterlaus, D. Pescia, and H. Melchior, Science **290**, 492 (2000).
[2] W. K. Hiebert, A. Stankiewicz, and M. R. Freeman, Phys. Rev. Lett. **79**, 1134 (1997).
[3] Th. Gerrits, H. A. M. van den Berg, J. Hohlfeld, L. Bär, and Th. Rasing, Nature (London) **418**, 509 (2002).
[4] E. Beaurepaire, J.-C. Merle, A. Daunois, and J.-Y. Bigot, Phys. Rev. Lett. **76**, 4250 (1996).
[5] B. Koopmans, M. van Kampen, J. T. Kohlhepp, and W. J. M. de Jonge, Phys. Rev. Lett. **85**, 844 (2000).
[6] L. Guidoni, E. Beaurepaire, and J.-Y. Bigot, Phys. Rev. Lett. **89**, 017401 (2002).
[7] M. van Kampen, C. Jozsa, J. T. Kohlhepp, P. LeClair, L. Lagae, W. J. M. de Jonge, and B. Koopmans, Phys. Rev. Lett. **88**, 227201 (2002).
[8] J. Hohlfeld, E. Matthias, R. Knorren, and K. H. Bennemann, Phys. Rev. Lett. **78**, 4861 (1997).
[9] M. Aeschlimann, M. Bauer, S. Pawlik, W. Weber, R. Burgermeister, D. Oberli, and H. C. Siegmann, Phys. Rev. Lett. **79**, 5158 (1997).
[10] A. Scholl, L. Baumgarten, R. Jacquemin, and W. Eberhardt, Phys. Rev. Lett. **79**, 5146 (1997).
[11] A. V. Kimel, A. Kirilyuk, P. A. Usachev, R. V. Pisarev, A. M. Balbashov, and Th. Rasing, Nature (London) **435**, 655 (2005).
[12] F. Hansteen, A. Kimel, A. Kirilyuk, and Th. Rasing, Phys. Rev. Lett. **95**, 047402 (2005).
[13] G. Zhang, W. Hübner, E. Beaurepaire, and J.-Y. Bigot, in *Spin Dynamics in Confined Magnetic Structures I*, edited by B. Hillebrands and K. Ounadjela (Springer, Berlin, 2002) Vol. 83, p. 245.
[14] J.-Y. Bigot, M. Vomir, and E. Beaurepaire, Nature Phys. **5**, 515 (2009).
[15] U. Bovensiepen, Nature Phys. **5**, 461 (2009).
[16] J.-Y. Bigot, M. Vomir, L. H. F. Andrade, and E. Beaurepaire, Chem. Phys. **318**, 137 (2005).
[17] G. Ju, A. V. Nurmikko, R. F. C. Farrow, R. F. Marks, M. J. Carey, and B. A. Gurney, Phys. Rev. Lett. **82**, 3705 (1999).
[18] M. Vomir, L. H. F. Andrade, L. Guidoni, E. Beaurepaire, and J.-Y. Bigot, Phys. Rev. Lett. **94**, 237601 (2005).
[19] A. V. Scherbakov, A. S. Salasyuk, A. V. Akimov, X. Liu, M. Bombeck, C. Brüggemann, D. R. Yakovlev, V. F. Sapega, J. K. Furdyna, and M. Bayer, Phys. Rev. Lett. **105**, 117204 (2010).
[20] H. T. Grahn, H. J. Maris, and J. Tauc, IEEE J. Quantum Electron. **25**, 2562 (1989).
[21] O. B. Wright and V. E. Gusev, IEEE Trans. Ultrason. Ferroelectr. Freq. Control **42**, 331 (1995).
[22] O. B. Wright, B. Perrin, O. Matsuda, and V. E. Gusev, Phys. Rev. B **78**, 024303 (2008).
[23] C. Thomsen, J. Strait, Z. Vardeny, H. J. Maris, J. Tauc, and J. J. Hauser, Phys. Rev. Lett. **53**, 989 (1984).
[24] C. Thomsen, H. T. Grahn, H. J. Maris, and J. Tauc, Phys. Rev. B **34**, 4129 (1986).
[25] T. Saito, O. Matsuda, and O. B. Wright, Phys. Rev. B **67**, 205421 (2003).
[26] L. Thevenard, E. Peronne, C. Gourdon, C. Testelin, M. Cubukcu, E. Charron, S. Vincent, A. Lemaître, and B. Perrin, Phys. Rev. B **82**, 104422 (2010).
[27] V. V. Temnov, U. Woggon, J. Dintinger, E. Devaux, and T. W. Ebbesen, Opt. Lett. **32**, 1235 (2007).
[28] H.-N. Lin, R. J. Stoner, H. J. Maris, and J. Tauc, J. Appl. Phys. **69**, 3816 (1991).
[29] C.-K. Sun, F. Vallée, L. H. Acioli, E. P. Ippen, and J. G. Fujimoto, Phys. Rev. B **50**, 15 337 (1994).
[30] Parameters used in the calculation: $\gamma = 6 \times 10^3$ Jm^{-3} K^{-2} in $C_e = \gamma T_e$ [4], $\kappa_e = 91$ Wm^{-1} K^{-1} [25], $\rho = 8.91 \times 10^3$ kg m^{-3}, $v = 4.08 \times 10^3$ ms^{-1}, $\beta = 1.3 \times 10^{-5}$ K^{-1}, $B = 1.8 \times 10^{11}$ Nm^{-2} [31], and $\lambda_s = -3.3 \times 10^{-5}$ [32].

$C_l = 2.2 \times 10^6$ Jm^{-3} K^{-1}, $g_{el} = 7.0 \times 10^{17}$ Wm^{-3} K^{-1}, and $g_{sl} = 0.3 \times 10^{17}$ Wm^{-3} K^{-1} [4], $g_{es} = 5.6 \times 10^{17}$ Wm^{-3} K^{-1}. $C_s(T_s) = m_1(1 - T_s/T_c)^{0.1} + m_2$, where $m_1 = -2.15 \times 10^6$ Jm^{-3} K^{-1} and $m_2 = 2.38 \times 10^6$ Jm^{-3} K^{-1} under the condition of $T_s < T_c$ [33].

[31] F. Luo, X.-R. Chen, L.-C. Cai, and Q. Wu, J. At. Mol. Sci. **2**, 10 (2011).

[32] S. Chikazumi, *Physics of Ferromagnetism* (Clarendon, Oxford, 1997), 2nd ed., p. 361.

[33] D. L. Connelly, J. S. Loomis, and D. E. Mapother, Phys. Rev. B **3**, 924 (1971).

[34] W. Reim and J. Schoenes, in *Ferromagnetic Materials*, edited by K. H. J. Buschow (North-Holland, Amsterdam, 1990), Vol. 5, p. 133.

[35] P. M. Oppeneer, in *Handbook of Magnetic Materials*, edited by K. H. J. Buschow (Elsevier, Amsterdam, 2006), Vol. 13, p. 294.

[36] T. L. Gilbert, IEEE Trans. Magn. **40**, 3443 (2004).